

Orographically Anchored El Niño Effect on Summer Rainfall in Central China

KAIMING HU

State Key Laboratory of Numerical Modeling for Atmospheric Sciences and Geophysical Fluid Dynamics, and Center for Monsoon System Research, Institute of Atmospheric Physics, Chinese Academy of Sciences, Beijing, China

SHANG-PING XIE

Scripps Institution of Oceanography, University of California, San Diego, La Jolla, California, and Physical Oceanography Laboratory, Ocean University of China, and Qingdao National Laboratory for Marine Science and Technology, Qingdao, China

GANG HUANG

State Key Laboratory of Numerical Modeling for Atmospheric Sciences and Geophysical Fluid Dynamics, and Center for Monsoon System Research, Institute of Atmospheric Physics, Chinese Academy of Sciences, Beijing, Laboratory for Regional Oceanography and Numerical Modeling, Qingdao National Laboratory for Marine Science and Technology, Qingdao, and University of Chinese Academy of Sciences, Beijing, China

(Manuscript received 12 May 2017, in final form 2 September 2017)

ABSTRACT

Year-to-year variations in summer precipitation have great socioeconomic impacts on China. Historical rainfall variability over China is investigated using a newly released high-resolution dataset. The results reveal summer-mean rainfall anomalies associated with ENSO that are anchored by mountains in central China east of the Tibetan Plateau. These orographically anchored hot spots of ENSO influence are poorly represented in coarse-resolution datasets so far in use. In post-El Niño summers, an anomalous anticyclone forms over the tropical northwest Pacific, and the anomalous southwesterlies on the northwest flank cause rainfall to increase in mountainous central China through orographic lift. At upper levels, the winds induce additional adiabatic updraft by increasing the eastward advection of warm air from Tibet. In post-El Niño summers, large-scale moisture convergence induces rainfall anomalies elsewhere over flat eastern China, which move northward from June to August and amount to little in the seasonal mean.

1. Introduction

Summer is the rainy season in China brought about by the East Asian summer monsoon (Tao and Chen 1987). Devastating floods and droughts that have occurred frequently during summer in China have motivated a search for useful predictors. While ENSO is widely used as an important predictor (Fu and Ye 1988; Huang and Wu 1989; Wang et al. 2000; Wu et al. 2009; Li et al. 2016; Zhang et al. 2016), the correlation of summer rainfall with ENSO is weak over China (Shen and Lau 1995; Xie et al. 2009), and the pattern is not well defined and varies

among interdecadal epochs (Chang et al. 2000; Wang 2002; Wu and Wang 2002) and across different studies (Huang and Wu 1989; Shen and Lau 1995). Unlike rainfall, the summer atmospheric circulation in East Asia shows a robust relationship with ENSO (Zhang et al. 1996; Wang et al. 2000). A low-level anomalous anticyclone over the tropical northwest Pacific often develops in El Niño winter and persists into the following summer (Wang et al. 2000; Yang et al. 2007; Xie et al. 2009). The anomalous anticyclone strengthens the northward vapor transport from the tropics to China, and is considered to be an important source of predictability for Chinese summer rainfall (Wang et al. 2013; Ma et al. 2017). Seasonal prediction of China rainfall is, however, of limited

Corresponding author: Gang Huang, hg@mail.iap.ac.cn

DOI: 10.1175/JCLI-D-17-0312.1

© 2017 American Meteorological Society. For information regarding reuse of this content and general copyright information, consult the [AMS Copyright Policy](http://www.ametsoc.org/PUBSReuseLicenses) (www.ametsoc.org/PUBSReuseLicenses).

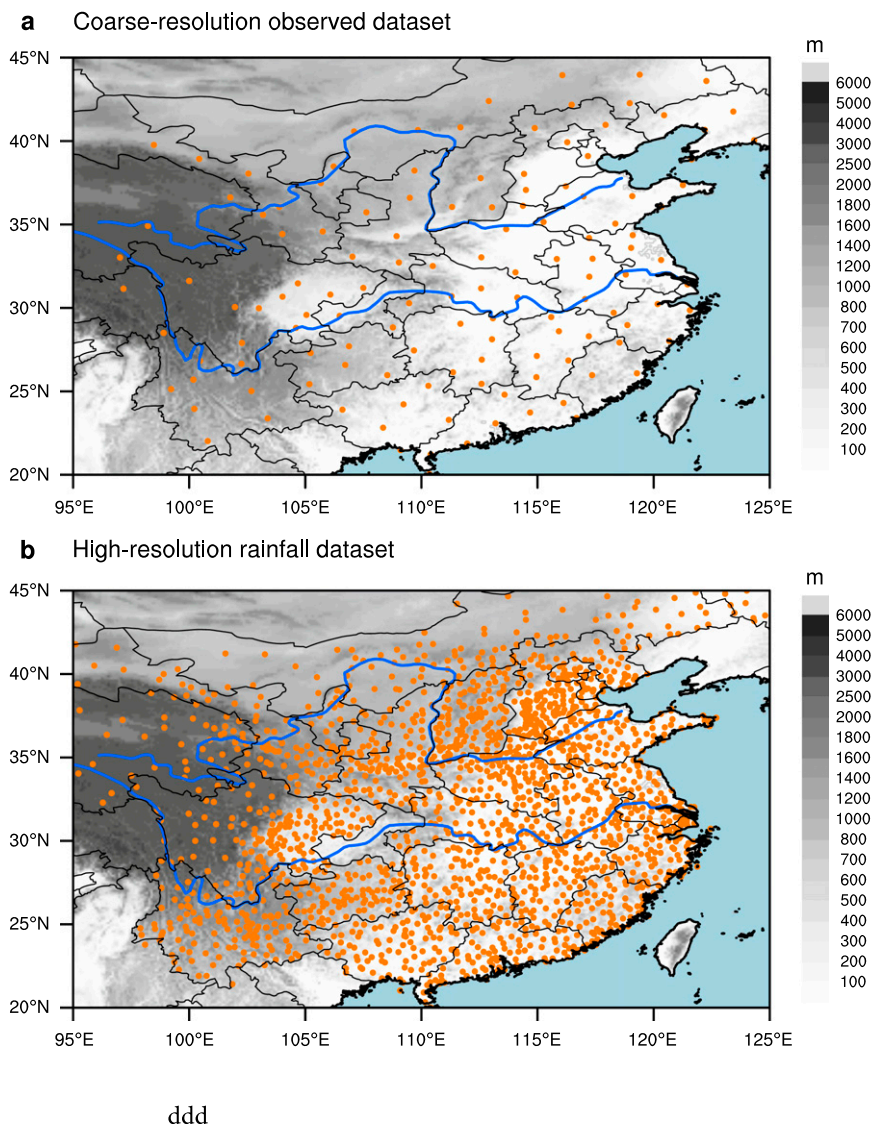


FIG. 1. The distribution of stations (orange dots) in (a) a coarse-resolution observed dataset with 160 stations in wide use until now and (b) a new high-resolution rainfall dataset used in this study, superimposed on elevation (gray shading; m). Blue lines mark the Yellow and Yangtze Rivers.

skill at best (Yim et al. 2016) because of such complicating factors as atmospheric internal variability (Kosaka et al. 2012), diversity in ENSO evolution (Zhang et al. 2016), and intraseasonal variability (Ye and Lu 2011).

Although the pattern of China summer rainfall anomalies associated with ENSO is not well defined, the enhanced northward vapor transport from tropical oceans to China in the post-El Niño summer is widely recognized and robust (Wang et al. 2000; Xie et al. 2009). In central China, there are several east-west-oriented mountain ranges, including the Wushans, the Bashans, the Qinlins, and the Loess Plateau, which extend from

the eastern foothills of the Tibetan Plateau to about 113°E, and rise above 2000 m above sea level. When the northward flows meet these mountain ranges, orographic lift may cause rainfall. The orographic effect on summer rainfall prediction has not been explored in the literature, possibly because rainfall datasets widely used in previous studies (Fig. 1a) are too coarse to resolve the mountains. Recently, the China Meteorological Data Service Center (<http://data.cma.cn/en>) released a high-resolution rainfall dataset (Fig. 1b), which enables us to investigate the role of orography in ENSO impact on rainfall.

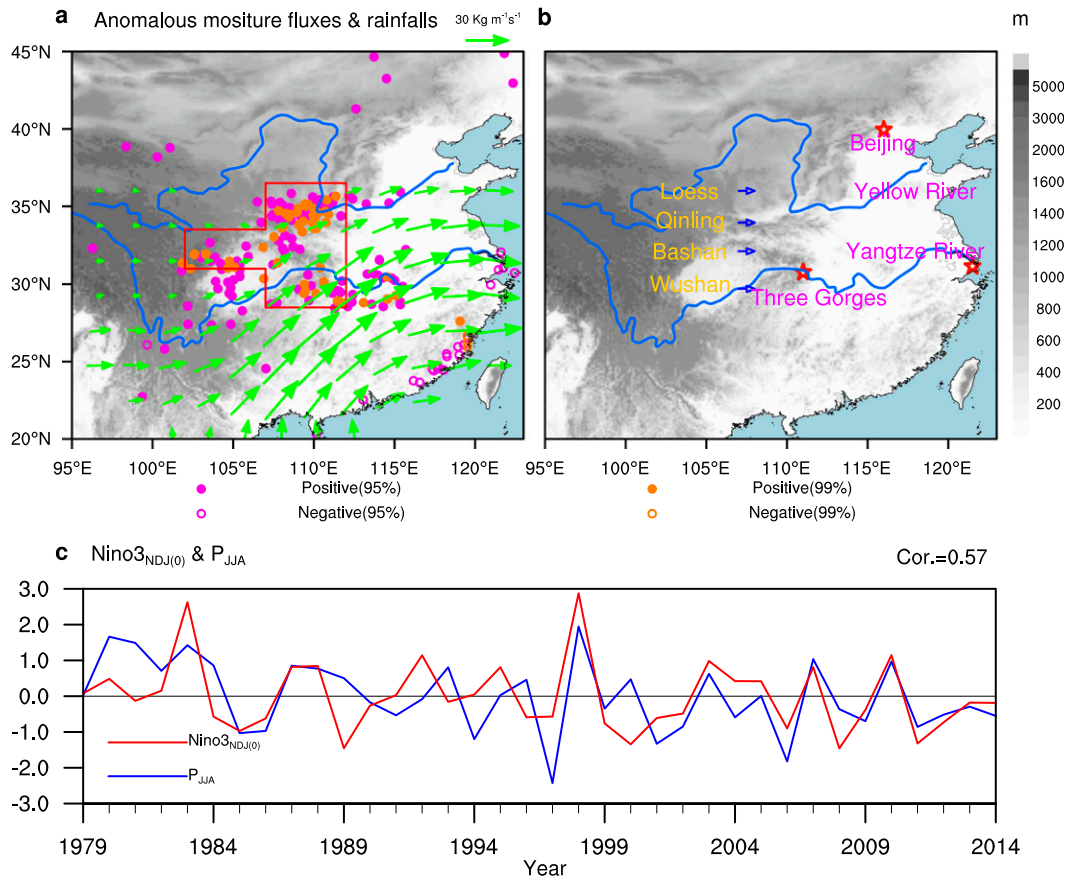


FIG. 2. Relationship between China summer-mean rainfall and ENSO. (a) The correlations (dots and circles) of JJA [following summer from NDJ(0)] mean rainfall and the regressions (vectors; shown only exceeding the 95% confidence level) of vertically integrated (from the surface to 200 hPa) moisture flux with NDJ(0) Niño-3 SST index during 1979–2014. (b) Geographic names of regions. (c) The normalized JJA rainfalls (blue line) averaged in the red polygon in (a) and the NDJ(0) Niño-3 SST index (red line). The gray shading in (a) and (b) denotes the topography (m). The magenta and orange dots (circles) represent positive (negative) correlations exceeding the 95% and the 99% confidence levels, respectively.

2. Data

The newly released high-resolution precipitation dataset contains 2400 observations in China (Fig. 1b). The time resolution is daily and the earliest record goes back to 1 January 1951. The number of stations increases gradually from 165 in 1951 to 2298 in 1979. After 1979, the spatial resolution is high enough to capture the orographic effect on rainfall. After excluding the stations with more than five missing-value days in a month, we retain 2163 stations. The monthly mean winds, air temperature, and vertical integral of moisture fluxes are derived from the latest global atmospheric reanalysis produced by the European Centre for Medium-Range Weather Forecasts, which has a horizontal resolution of $0.75^\circ \times 0.75^\circ$ and 37 vertical levels from 1000 hPa to 1 hPa (ERA-Interim; Dee et al. 2011). We use the global gridded monthly sea surface temperature dataset of the Met

Office Hadley Centre (Rayner et al. 2003), which has a resolution of $1^\circ \times 1^\circ$ and is available from 1870 forward. We use November–January (NDJ) mean Niño-3 (5°S – 5°N , 90° – 150°W) sea surface temperature (SST) index to denote the annual variations of ENSO, and similar results are obtained when the NDJ Niño-3.4 index is used (results are not shown).

3. Orographic effect in post-ENSO summers

Figure 2a shows the stations with significant correlation between June–August (JJA) mean rainfall and the November–January mean from the preceding year [NDJ(0)] Niño-3 SST index during 1979–2014. Among 2163 stations, 183 display significant positive correlation (above the 95% confidence level) but only 28 stations show significant negative correlation (above

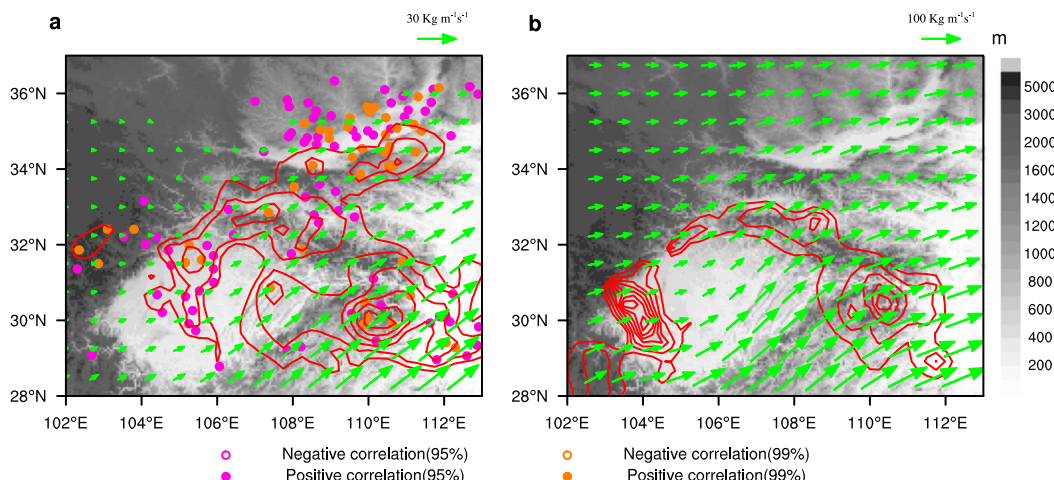


FIG. 3. Orographic effect on rainfall. (a) JJA anomalies of rainfall (shown only above 0.5 mm day^{-1} , with contour intervals at 0.2 mm day^{-1}) and vertically integrated moisture fluxes (vectors; exceeding the 95% confidence level) regressed onto normalized NDJ(0) Niño-3 SST index. (b) Climatological JJA rainfall (shown only above 7 mm day^{-1} , with contour intervals at 0.5 mm day^{-1}) and vertically integrated moisture fluxes (vectors) from 1979 to 2014. The dots and circles in (a) are as in Fig. 2a.

the 95% confidence level), indicating that China is prone to floods in post-El Niño summers. Statistical significance here is evaluated with the two-sided Student's t test. Most stations with significant positive correlation, some above the 99% confidence level, are distributed along the east-west-oriented mountain ranges east of Tibet and on the south face of the Loess Plateau, in conjunction with prominent southwesterly vapor flux anomalies (Fig. 2a). Here the vapor flux anomalies are the regressions of JJA mean vapor fluxes on the normalized Niño-3 SST index during 1979–2014. Specifically, in the mountainous area of central China (the red polygon in Fig. 2a), 103 out of 210 stations show positive correlations above the 95% confidence level. The correlation between the JJA rainfalls averaged in the red polygon in Fig. 2a and NDJ(0) Niño-3 SST index amounts to 0.57 (above the 99% confidence level) during 1979–2014. Here, P_{JJA} is calculated by averaging JJA rainfall (on a $0.25^\circ \times 0.25^\circ$ grid using bilinear interpolation of station data) in the red polygon in Fig. 2a ($28.5^\circ\text{--}36.5^\circ\text{N}$, $107^\circ\text{--}112^\circ\text{E}$ and $31^\circ\text{--}33.5^\circ\text{N}$, $102^\circ\text{--}107^\circ\text{E}$). Most post-El Niño years (1983, 1987, 1988, 1998, 2003, 2007, and 2010) coincide with above-normal summer rainfall in the red polygon in Fig. 2a, while most post-La Niña years (1985, 1997, 2001, 2006, 2008, 2009, and 2010) feature below-normal rainfall (Fig. 2c). Thus, JJA rainfall in the mountainous area of central China is closely related to ENSO events in the preceding winter. The relationship is consistent with local forecasters' experience (Zhao et al. 2013) that rainfall at some stations in

mountainous center China tends to be above normal in post-El Niño summers, but the underlying mechanism is unclear.

This relationship with ENSO is important for more than 100 million people living in this mountainous area. Abnormal rainfall on steep mountain slopes can cause landslides and floods. Two of the largest rivers in China, the Yellow and the Yangtze, flow through the region. The world's largest dam, the Three Gorges, is there too (Fig. 2b), and excessive rainfall could put the dam in danger. Great floods (Liu 2015) happened in summers of 1981, 1983, 1988, 1998, 2000, 2002, 2007, 2010, and 2012, most preceded by El Niño events. The relationship with El Niño can help predict rainfall in this area several months in advance.

The pattern of rainfall anomalies in post-El Niño summers is in broad agreement with the hypothesis of orographic effect. They are locally enhanced along the ridges of the Wushans, the Bashans, and Qinlings, as the anomalous southwesterly winds impinge upon the mountain ranges (Fig. 3a). On the south face of the Loess Plateau (35°N , 110°E), rainfall anomalies are highly significant (dots in Fig. 3a), albeit moderate in magnitude. The climatological distribution of JJA rainfall also shows local enhancements along the ridge of the mountains facing the southwesterly winds (Fig. 3b), in support of the orographic effect.

Over eastern China, the summer climatological rainband is not stationary but marches northward from June to August (Tao and Chen 1987). Figure 4 shows the evolution of the rainfall-ENSO correlation from June to

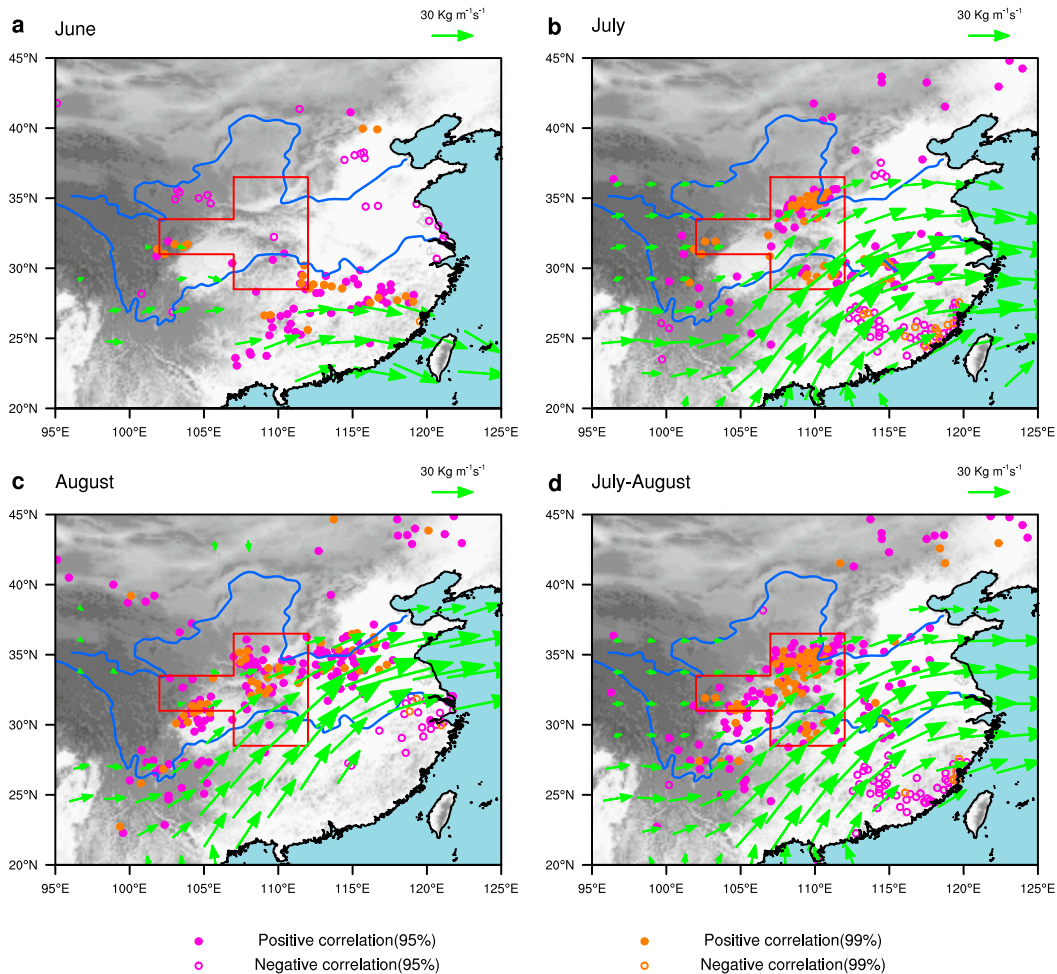


FIG. 4. The correlations (dots and circles) of monthly mean rainfall and the regressions of monthly mean vertically integrated (from the surface to 200 hPa) moisture flux (vectors; shown only exceeding the 95% confidence level) for (a) June, (b) July, (c) August, and JJA mean with NDJ(0) Niño-3 SST index during 1979–2014. The dots and circles are same as Fig. 2a, but for monthly mean rainfall.

August, together with the moisture flux anomalies regressed upon the normalized NDJ(0) Niño-3 index. Over relatively flat eastern China, rainfall increases in a narrow zonal band in each month of a post-El Niño summer. This band of increased rainfall (filled cycles) is not stationary but advances northward from 28°N in June to 36°N in August. This mobile band of high rainfall–ENSO correlation has been noted previously (Ye and Lu 2011), and here we show that it is due to the large-scale moisture convergence on the northern flank of the northwestern Pacific anomalous anticyclone. The anomalous vapor fluxes associated with ENSO are not fixed geographically within the summer, with the northern flank marching northward from 27°N in June to 35°N in July and 38°N in August. Associated with the northward advance of the conduit of the southwesterly anomalous vapor fluxes, the

large-scale convergence (Fig. 5) causes rainfall to increase on the northern flank of the conduit, while the divergence causes rainfall to decrease on the southern flank.

In the seasonal mean, the mobile band of high rainfall correlation in monthly maps averages out over flat eastern China. This explains why the relationship of seasonal-mean rainfall variability to ENSO is not robust in the literature (Shen and Lau 1995; Ye and Lu 2011), which focuses almost exclusively on the seasonal means. The stationary orographic effect dominates the summer-mean rainfall variability associated with ENSO. This orographic effect has been overlooked in coarse-resolution datasets but is obvious in our high-resolution analysis as stations of high correlation are many and clustered around major orographic features.

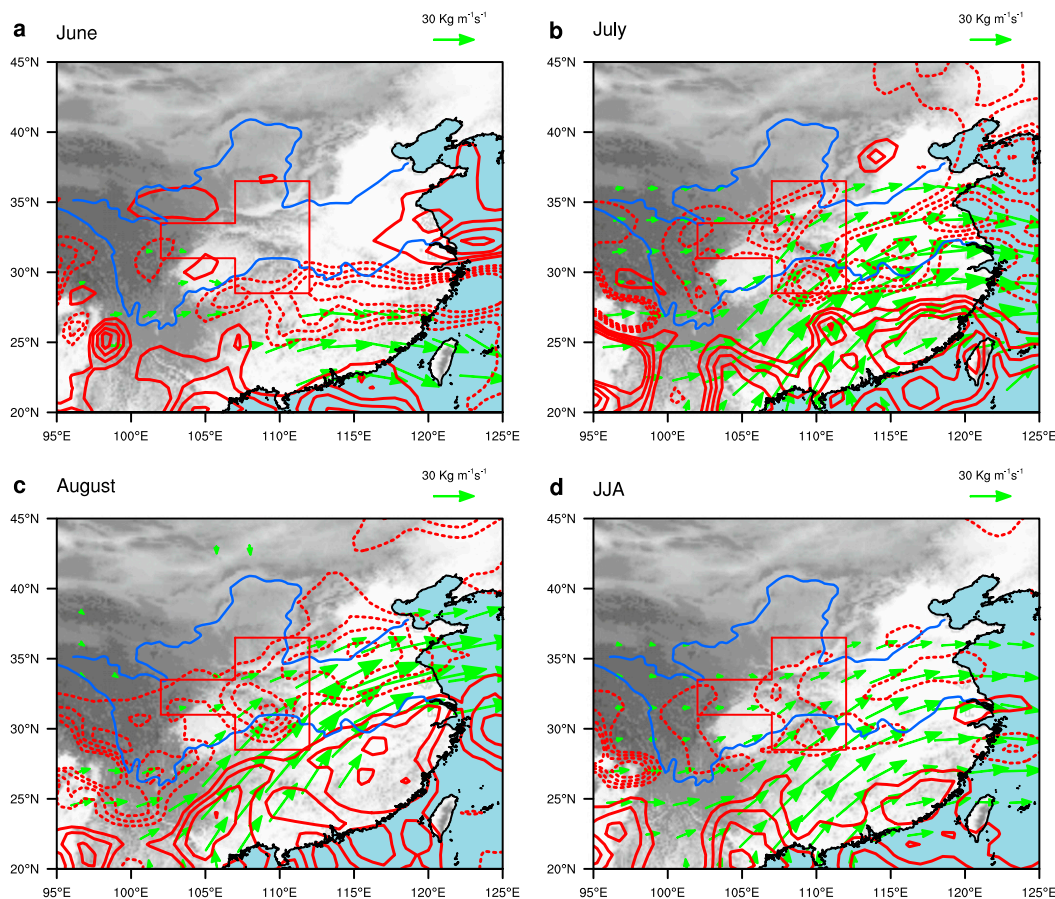


FIG. 5. The regression of vertically integrated (from the surface to 200 hPa) moisture fluxes (vectors) and their divergence (shown only above 0.3 mm day^{-1} ; contours at 0.2 mm day^{-1} intervals; the solid and dashed contours refer to divergence and convergence anomalies) in (a) June, (b) July, (c) August, and (d) the JJA mean onto normalized NDJ(0) Niño-3 SST index.

4. Mechanisms for ENSO impact

The southwesterly vapor flux anomalies in July and August are mainly caused by El Niño-induced anomalous circulation at low and middle levels. Figures 6a and 6b show the El Niño-induced July–August (JA) mean circulation anomalies at 850 and 500 hPa regressed upon the normalized NDJ(0) Niño-3 SST index, respectively. At 850 hPa, a prominent anomalous anticyclone extends from the tropical northwest Pacific to the eastern flank of the Tibetan Plateau (Fig. 6a). The strong southerly wind anomalies along the eastern flank of the Tibetan Plateau bring water vapor from the tropics into central China. At 500 hPa, the anomalous anticyclone extends farther westward than at 850 hPa, with anomalous southwesterlies over the Tibetan Plateau (Fig. 6b). In the upper troposphere, there are significant westerly wind anomalies over the Tibetan Plateau (Fig. 6c). Both upper-level

westerly anomalies (Lau et al. 2005; Qu and Huang 2012) and low-level anticyclonic anomalies (Wang et al. 2000; Du et al. 2009; Wu et al. 2010; Xie et al. 2016) are mainly caused by lingering SST anomalies in the tropical Indo-western Pacific sector (Fig. 6a) following an El Niño event.

In JA climatology, air temperature over the Tibetan Plateau is higher than the surrounding regions at the same altitudes (Figs. 6b,c). The southwesterly anomalies in the midtroposphere (Fig. 6b) and westerly anomalies in the upper troposphere (Fig. 6c) over the Tibetan Plateau can transport warm air downstream, inducing significant upward motion (Sampe and Xie 2010) in the midtroposphere over central China (Fig. 6c). Indeed, anomalous upward motion at 500 hPa in the red polygon is associated with strong anomalous warm temperature advection (Fig. 6b).

We used the omega equation (Kosaka and Nakamura 2010) to diagnose the vertical motion anomalies:

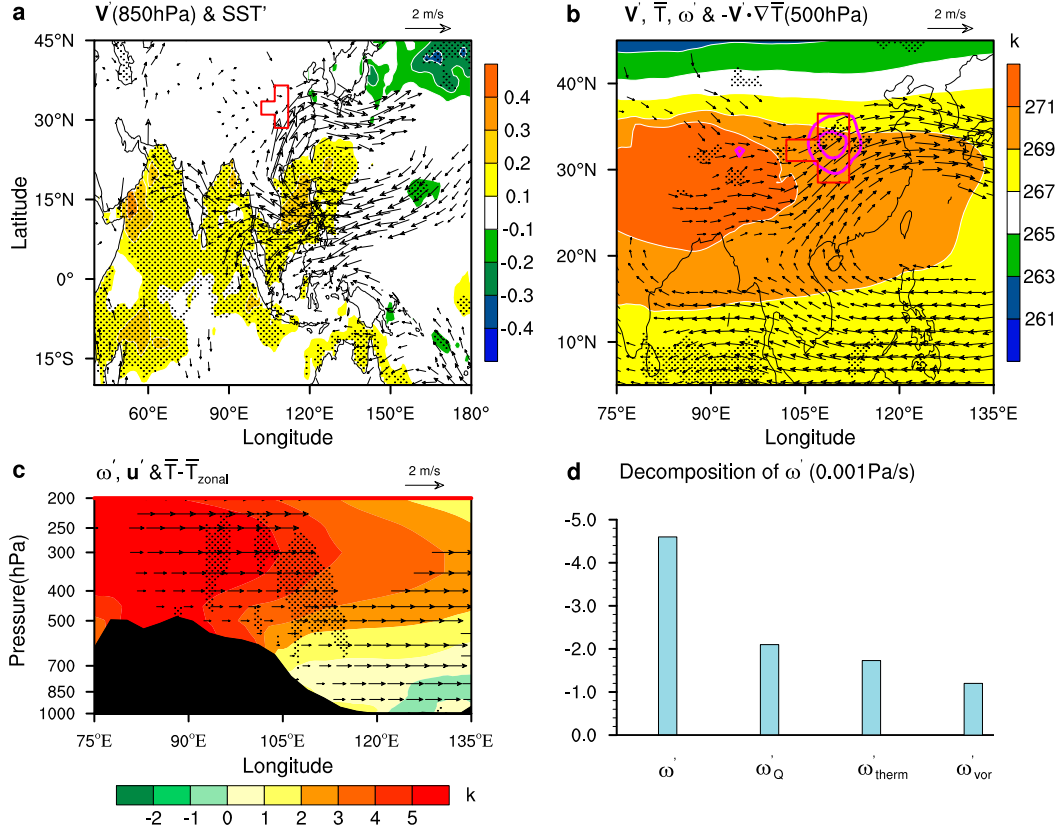


FIG. 6. El Niño-related JJA averaged atmospheric circulation and SST anomalies. (a) Wind anomalies (vectors) at 850 hPa and SST anomalies (color shading, for shades passing the 95% confidence level; K). (b) Anomalous winds (vectors), temperature advection (above 0.1 K day^{-1} ; magenta contours at interval of 0.05 K day^{-1}), omegas (hatching), and climatological temperatures (color shading; K) at 500 hPa. (c) Longitude–height section of 30° – 35°N averaged anomalous zonal winds (vectors), vertical velocity (ω' ; hatching), and climatological temperature deviation from zonal mean (color shading; K). (d) The decomposition of omega anomaly in the red polygon. In (a)–(d), the anomalies are the regressions onto NDJ(0) Niño-3 SST index. Only the anomalous winds and negative ω exceeding the 95% confidence level are shown.

$$\omega' = \underbrace{\left(\nabla^2 + \frac{f^2}{\sigma^2} \frac{\partial^2}{\partial P^2} \right)^{-1} \frac{f}{\sigma} \frac{\partial}{\partial P} [\bar{\mathbf{u}} \cdot \nabla \zeta' + \mathbf{u}' \cdot \nabla (f + \bar{\zeta})]}_{\omega_{\text{vor}}} + \underbrace{\left(\nabla^2 + \frac{f^2}{\sigma^2} \frac{\partial^2}{\partial P^2} \right)^{-1} \frac{R}{\sigma P} \nabla^2 (\bar{\mathbf{u}} \cdot \nabla T' + \mathbf{u}' \cdot \nabla \bar{T})}_{\omega_{\text{therm}}} + \underbrace{\left[- \left(\nabla^2 + \frac{f^2}{\sigma^2} \frac{\partial^2}{\partial P^2} \right)^{-1} \frac{R}{\sigma P c_p} \nabla^2 Q \right]}_{\omega_Q}$$

where the overbar and prime indicate climatological mean quantities for July–August and the regressed anomalies, respectively. Also, $\sigma = (R/P)(RT/c_p P - dT/dP)$ denotes the static stability, ζ is relative vorticity, f is the Coriolis parameter, R is the gas constant, T is the air temperature,

P is the atmospheric pressure, $\mathbf{u} = (u, v)$ is the horizontal wind velocity, c_p is specific heat at constant pressure, and Q is diabatic heating. The result indicates that the vertical motion anomaly at 500 hPa in the red polygon is due 42% to diabatic heating ω_Q , 34% to horizontal temperature advection ω_{therm} , and 24% to the vertical difference of vorticity horizontal advection ω_{vor} (Fig. 6d). Diabatic heating is closely coupled to rainfall and vertical motion and should be considered as a feedback, instead of an external forcing. Thus, the hot spots of El Niño influence in the red polygon over central China is due not only to low-level orographic lift but also to midtropospheric updraft induced by the intensified warm advection anchored by the Tibetan Plateau. The anomalous warm air temperature advection may explain positive rainfall anomalies that extend outside the mountain ranges over central China; for example, positive anomalies in the flat region around 105° – 106°E .

While the midtropospheric thermal advection is of a large scale, mountain ranges modulate rainfall and vertical motion. Our results show that the large-scale circulation is also in favor of anomalous upward motion in addition to orographic lifting in the presence of enhanced low-level moisture transport.

5. Summary and discussion

We have uncovered a hitherto unknown pattern of El Niño–induced summer rainfall variability over China that is anchored by mountain ranges on the eastern flank of the Tibetan Plateau. In post–El Niño summers, low-level anomalous southwesterlies carry moist air from the south, force orographic lift upon impinging on these narrow mountain ranges, and cause rainfall. Aiding this low-level orographic lifting effect, the upper-level anomalous westerlies induce adiabatic updraft by intensifying the warm advection from the climatological temperature maximum from Tibet.

In addition to the stationary orographic effect, our monthly analysis has also identified narrow bands of rainfall anomalies over flat eastern China associated with the large-scale moisture convergence. As the conduit of the southwesterly moisture transport on the northwest flank of the El Niño–induced anomalous anticyclone advances northward from June to August, the large-scale circulation convergence and resultant bands of rainfall anomalies move northward from June to August. As the mobile bands of rainfall anomalies average out over the course of a summer, the JJA mean rainfall anomalies are dominated by the orographic effect over mountainous central China. The results explain why previous studies did not find a well-defined summer-mean rainfall pattern associated with ENSO in coarse-resolution datasets that do not adequately resolve the orographic effect (Shen and Lau 1995; Xie et al. 2009).

Previous studies show that the relationship between the northwestern Pacific anticyclone and ENSO is not stable on multidecadal scales (Wang et al. 2008; Xie et al. 2010; Huang et al. 2010). Using a coarse-resolution (160 stations in China) but long-term (1951–2014) rainfall dataset, we found that the relationship between NDJ(0) Niño-3 SST index and the following summer [JJA(1)] rainfall index in central China becomes tighter after the late 1970s (results are not shown), in agreement with the observation that ENSO's impact on the northwestern Pacific anticyclone strengthens after the late 1970s (Wang et al. 2008; Xie et al. 2010; Huang et al. 2010). As climate warms with increasing greenhouse forcing (Held and Soden 2006), increased water vapor content in the atmosphere is likely to elevate the risk of ENSO-induced floods in this densely populated region if

the circulation anomalies over East Asia do not change. The projected increase in extreme ENSO events (Cai et al. 2015) may further exacerbate the risk. In addition, it is noted that some strong ENSO events, especially some strong La Niña events (e.g., 1988/89 and 2000/01), did not correspond to strong summer rainfall anomalies in mountainous central China, which deserves future study.

Acknowledgments. We thank Xia Qu and Lin Wang for helpful discussions. This work is supported by the Natural Science Foundation of China (41775086 and 41661144016), the Public Science and Technology Research Funds Projects of Ocean (201505013), and the U.S. National Science Foundation (1637450). The authors declare no competing interests.

REFERENCES

- Cai, W., and Coauthors, 2015: ENSO and greenhouse warming. *Nat. Climate Change*, **5**, 849–859, <https://doi.org/10.1038/nclimate2743>.
- Chang, C. P., Y. S. Zhang, and T. Li, 2000: Interannual and interdecadal variations of the East Asian summer monsoon and tropical Pacific SSTs. Part I: Roles of the subtropical ridge. *J. Climate*, **13**, 4310–4325, [https://doi.org/10.1175/1520-0442\(2000\)013<4310:IAIVOT>2.0.CO;2](https://doi.org/10.1175/1520-0442(2000)013<4310:IAIVOT>2.0.CO;2).
- Dee, D., and Coauthors, 2011: The ERA-Interim reanalysis: Configuration and performance of the data assimilation system. *Quart. J. Roy. Meteor. Soc.*, **137**, 553–597, <https://doi.org/10.1002/qj.828>.
- Du, Y., S.-P. Xie, G. Huang, and K. Hu, 2009: Role of air–sea interaction in the long persistence of El Niño–induced north Indian Ocean warming. *J. Climate*, **22**, 2023–2038, <https://doi.org/10.1175/2008JCLI2590.1>.
- Fu, C., and D. Ye, 1988: The tropical very low-frequency oscillation on interannual scale. *Adv. Atmos. Sci.*, **5**, 369–388, <https://doi.org/10.1007/BF02656760>.
- Held, I. M., and B. J. Soden, 2006: Robust responses of the hydrological cycle to global warming. *J. Climate*, **19**, 5686–5699, <https://doi.org/10.1175/JCLI3990.1>.
- Huang, G., K. Hu, and S.-P. Xie, 2010: Strengthening of tropical Indian Ocean teleconnection to the northwest Pacific since the mid-1970s: An atmospheric GCM study. *J. Climate*, **23**, 5294–5304, <https://doi.org/10.1175/2010JCLI3577.1>.
- Huang, R., and Y. Wu, 1989: The influence of ENSO on the summer climate change in China and its mechanism. *Adv. Atmos. Sci.*, **6**, 21–32, <https://doi.org/10.1007/BF02656915>.
- Kosaka, Y., and H. Nakamura, 2010: Mechanisms of meridional teleconnection observed between a summer monsoon system and a subtropical anticyclone. Part I: The Pacific–Japan pattern. *J. Climate*, **23**, 5085–5108, <https://doi.org/10.1175/2010JCLI3413.1>.
- , J. S. Chowdary, S.-P. Xie, Y.-M. Min, and J.-Y. Lee, 2012: Limitations of seasonal predictability for summer climate over East Asia and the northwestern Pacific. *J. Climate*, **25**, 7574–7589, <https://doi.org/10.1175/JCLI-D-12-00009.1>.
- Lau, N. C., A. Leetmaa, M. J. Nath, and H. L. Wang, 2005: Influences of ENSO-induced Indo-western Pacific SST anomalies on extratropical atmospheric variability during the boreal summer. *J. Climate*, **18**, 2922–2942, <https://doi.org/10.1175/JCLI3445.1>.

- Li, L. F., W. H. Li, Q. H. Tang, P. F. Zhang, and Y. M. Liu, 2016: Warm season heavy rainfall events over the Huaihe River Valley and their linkage with wintertime thermal condition of the tropical oceans. *Climate Dyn.*, **46**, 71–82, <https://doi.org/10.1007/s00382-015-2569-2>.
- Liu, P.-G., 2015: Typical flood disasters in modern Shanxi history (in Chinese). *Northwest Hydropower*, **5**, 8–10.
- Ma, J., S.-P. Xie, and H. Xu, 2017: Intermember variability of the summer northwest Pacific subtropical anticyclone in the ensemble forecast. *J. Climate*, **30**, 3927–3941, <https://doi.org/10.1175/JCLI-D-16-0638.1>.
- Qu, X., and G. Huang, 2012: Impacts of tropical Indian Ocean SST on the meridional displacement of East Asian jet in boreal summer. *Int. J. Climatol.*, **32**, 2073–2080, <https://doi.org/10.1002/joc.2378>.
- Rayner, N. A., D. E. Parker, E. B. Horton, C. K. Folland, L. V. Alexander, D. P. Rowell, E. C. Kent, and A. Kaplan, 2003: Global analyses of sea surface temperature, sea ice, and night marine air temperature since the late nineteenth century. *J. Geophys. Res.*, **108**, 4407, <https://doi.org/10.1029/2002JD002670>.
- Sampe, T., and S.-P. Xie, 2010: Large-scale dynamics of the meiyubaiu rainband: Environmental forcing by the westerly jet. *J. Climate*, **23**, 113–134, <https://doi.org/10.1175/2009JCLI3128.1>.
- Shen, S., and K.-M. Lau, 1995: Biennial oscillation associated with the East Asian summer monsoon and tropical sea surface temperatures. *J. Meteor. Soc. Japan*, **73**, 105–124, https://doi.org/10.2151/jmsj1965.73.1_105.
- Tao, S.-Y., and L. X. Chen, 1987: A review of recent research on the East Asian summer monsoon in China. *Monsoon Meteorology*, C.-P. Chang and T. N. Krishnamurti, Eds., Oxford University Press, 60–92.
- Wang, B., R. G. Wu, and X. H. Fu, 2000: Pacific–East Asian teleconnection: How does ENSO affect East Asian climate? *J. Climate*, **13**, 1517–1536, [https://doi.org/10.1175/1520-0442\(2000\)013<1517:PEATHD>2.0.CO;2](https://doi.org/10.1175/1520-0442(2000)013<1517:PEATHD>2.0.CO;2).
- , J. Yang, and T. J. Zhou, 2008: Interdecadal changes in the major modes of Asian–Australian monsoon variability: Strengthening relationship with ENSO since the late 1970s. *J. Climate*, **21**, 1771–1789, <https://doi.org/10.1175/2007JCLI1981.1>.
- , B. Q. Xiang, and J.-Y. Lee, 2013: Subtropical high predictability establishes a promising way for monsoon and tropical storm predictions. *Proc. Natl. Acad. Sci. USA*, **110**, 2718–2722, <https://doi.org/10.1073/pnas.1214626110>.
- Wang, H., 2002: The instability of the East Asian summer monsoon–ENSO relations. *Adv. Atmos. Sci.*, **19**, 1–11, <https://doi.org/10.1007/s00376-002-0029-5>.
- Wu, B., T. Li, and T. Zhou, 2010: Relative contributions of the Indian Ocean and local SST anomalies to the maintenance of the western North Pacific anomalous anticyclone during the El Niño decaying summer. *J. Climate*, **23**, 2974–2986, <https://doi.org/10.1175/2010JCLI3300.1>.
- Wu, R. G., and B. Wang, 2002: A contrast of the East Asian summer monsoon–ENSO relationship between 1962–77 and 1978–93. *J. Climate*, **15**, 3266–3279, [https://doi.org/10.1175/1520-0442\(2002\)015<3266:ACOTEA>2.0.CO;2](https://doi.org/10.1175/1520-0442(2002)015<3266:ACOTEA>2.0.CO;2).
- Wu, Z. W., B. Wang, J. P. Li, and F.-F. Jin, 2009: An empirical seasonal prediction model of the East Asian summer monsoon using ENSO and NAO. *J. Geophys. Res.*, **114**, D18120, <https://doi.org/10.1029/2009JD011733>.
- Xie, S.-P., K. M. Hu, J. Hafner, H. Tokinaga, Y. Du, G. Huang, and T. Sampe, 2009: Indian Ocean capacitor effect on Indo-western Pacific climate during the summer following El Niño. *J. Climate*, **22**, 730–747, <https://doi.org/10.1175/2008JCLI2544.1>.
- , Y. Du, G. Huang, X.-T. Zheng, H. Tokinaga, K. Hu, and Q. Liu, 2010: Decadal shift in El Niño influences on Indo-western Pacific and East Asian climate in the 1970s. *J. Climate*, **23**, 3352–3368, <https://doi.org/10.1175/2010JCLI3429.1>.
- , Y. Kosaka, Y. Du, K. Hu, J. S. Chowdary, and G. Huang, 2016: Indo-western Pacific ocean capacitor and coherent climate anomalies in post-ENSO summer: A review. *Adv. Atmos. Sci.*, **33**, 411–432, <https://doi.org/10.1007/s00376-015-5192-6>.
- Yang, J. L., Q. Y. Liu, S.-P. Xie, Z. Y. Liu, and L. X. Wu, 2007: Impact of the Indian Ocean SST basin mode on the Asian summer monsoon. *Geophys. Res. Lett.*, **34**, L02708, <https://doi.org/10.1029/2006GL028571>.
- Ye, H., and R. Y. Lu, 2011: Subseasonal variation in ENSO-related East Asian rainfall anomalies during summer and its role in weakening the relationship between the ENSO and summer rainfall in eastern China since the late 1970s. *J. Climate*, **24**, 2271–2284, <https://doi.org/10.1175/2010JCLI3747.1>.
- Yim, S.-Y., B. Wang, and W. Xing, 2016: Peak-summer East Asian rainfall predictability and prediction. Part II: Extratropical East Asia. *Climate Dyn.*, **47**, 15–30, <https://doi.org/10.1007/s00382-015-2849-x>.
- Zhang, R., A. Sumi, and M. Kimoto, 1996: Impact of El Niño on the East Asian monsoon: A diagnostic study of the '86/87 and '91/92 events. *J. Meteor. Soc. Japan*, **74**, 49–62, https://doi.org/10.2151/jmsj1965.74.1_49.
- Zhang, W. J., and Coauthors, 2016: Unraveling El Niño's impact on the East Asian monsoon and Yangtze River summer flooding. *Geophys. Res. Lett.*, **43**, 11 375–11 382, <https://doi.org/10.1002/2016GL071190>.
- Zhao, Q., H. Yan, and L. Cheng, 2013: Characteristics of Shaanxi summer precipitation anomalies in ENSO developing and decaying stages (in Chinese). *J. Appl. Meteor. Sci.*, **24**, 495–503.